EFFECT OF MIXING CHAMBER STRUCTURE ON THE PERFORMANCE OF ADJUSTABLE EJECTOR

by

Zhong ZHOU[a], Yuze HAN[b], Zhi LI[a], Ningyu SUN[c], and Lijuan HE[a*]

[a]Inner Mongolia University of Science and Technology, Baotou, China
[b]Guilin University of Technology, Guangxi, China
[c]Huzhou Welion Technology Co., Ltd., Huzhou, China

Original scientific paper
https://doi.org/10.2298/TSCI240714229Z

The study employs numerical simulation method to analyze performance of an adjustable ejector, with a specific focus on the influence of the structure dimension of mixing chamber. The R41/R1234yf refrigerant is used as the working medium in the study. The primary and secondary flow inlets are set at the pressure of 1.4 MPa and 0.2 MPa, respectively, along with temperature of 353.15 K and 288.15 K corresponding. The outlet pressure of the ejector is 0.3 MPa. The simulation results show that optimal mixing chamber diameter within a range from 14.7 mm to 18.7 mm exists for obtaining peak adjustable ejector performance. Maximum entrainment ratio of 0.59 is obtained when cone diameter ratio is 65% and diameter of the mixing chamber is 15.7 mm. Furthermore, the optimal mixing chamber length within range from 24 mm to 220 mm exists for obtaining peak adjustable ejector performance. Maximum entrainment ratio of 0.624 is obtained when cone diameter ratio is 76% and length of the mixing chamber is 88 mm. Therefore, it is crucial during designing process of the mixing chamber to ensure the complete fluid mixture and minimal flow resistance.

Key words: *adjustable ejector, performance optimization, numerical simulation, mixing chamber dimensions, entrainment ratio*

Introduction

In response to the significant energy demands of conventional mechanical compression refrigeration systems, the integration of an ejector is introduced to increase energy efficiency [1-4]. The ejector operates on the following mechanism, high pressure primary flow passes through a convergent-divergent nozzle, achieving sonic speed at its throat and supersonic speed at its exit. In this process, the pressure of the primary flow is decreased, with its pressure energy being converted into kinetic energy. The primary flow at the nozzle outlet, characterized by lower static pressure, establishes a pressure difference with the secondary flow inlet, propelling the secondary flow into the suction chamber. Following this, the two fluids are mixed, lending to intense exchanges of mass, momentum and energy. As the velocity of the mixed fluid transitions from supersonic to subsonic, a shock wave is produced, causing the pressure

*Corresponding author, e-mail: zdlilyhe@163.com

increase and enter the diffuser. Within the diffuser, the kinetic energy of the mixed fluid is transformed into pressure energy. Then discharged through the ejector outlet, increasing the secondary flow pressure.

Wang *et al*. [5] investigated influence of mixing chamber structure of a vapor ejector on entrainment ratio. The results showed that entrainment ratio is significantly linked to variations in shock wave within the mixing chamber. Furthermore, there are optimal values for all parts of mixing chamber structure to achieve the maximum entrainment ratio. Jia and Wenjian [6] and Yan *et al*. [7] performed experiments on ejector-based refrigeration systems to obtain the influence of the ejector nozzle throat area on the system performance in refrigeration system. The results showed that the optimal throat area varies with operating conditions. The system can obtain the maximum cooling capacity and COP by adjusting the throat area to its optimal dimension. Varga *et al*. [8] employed CFD to investigate the influence of the area ratio between the nozzle throat and the mixing chamber cross-sectional area. The simulation results showed that the optimal area ratios vary with different operating conditions. To solve them, an adjustable cone was introduced at the primary flow inlet. By changing the position of the cone, the effective cross-sectional area of the nozzle throat was obtained in order to adjust the fluid flow rate. Consequently, the adjustment led to improvement in the ejector performance under a range of operating conditions.

Li *et al*. [9] investigated the performance characteristics of an ejector-expansion refrigeration cycle (EERC) utilizing R1234yf as the refrigerant within a constant-pressure mixing ejector configuration. The findings indicated that the R1234yf EERC outperformed the standard refrigeration cycle. This enhancement was especially notable under conditions of elevated condensing temperatures and reduced evaporation temperatures. Yang *et al*. [10] used the aerodynamic function method to establish a dynamic model of the mixture (R32/R245fa) ejector. Based on the designed structural size of the mixture ejector, the numerical simulation was conducted to analyze the characteristics of the mixture ejector. The simulation results showed that the entrainment ratio of the mixture (R32/R245fa) ejector was 78.95% higher than that of the pure refrigerant (R245fa) ejector. The above studies investigate the importance of the ejector structure. However, the influence of the mixing chamber structure on the performance of the adjustable ejector has not been studied. Given that both R41 and R1234yf refrigerants possess low ozone depletion potential and global warming potential, in this study, the R41/R1234yf mixed refrigerant is utilized as the working fluid to investigate the influence of the diameter and length of the mixing chamber on the performance of the adjustable ejector.

Physical model of an adjustable ejector

To adapt to different working conditions, an adjustable ejector has been designed. The flow area at the nozzle throat can be adjusted by horizontally moving the adjusting cone, thus enhancing the performance of the ejector. The design scheme effectively solves the problem that traditional ejectors cannot be adjusted promptly under variable working conditions. A 3-D adjustable ejector has been independently designed with the help of modeling software, and its structural dimensions are shown in fig. 1. Origin (0, 0, 0) of Cartesian co-ordinate system is located at the intersection of the axis of the adjustable cone and the inlet of the primary flow.

Considering the practical application of the adjustable ejector, the adjustable cone is designed as a conical surface. The structural parameters related to the design of the adjustable cone mainly include the cone top angle of 24°, the cone bottom diameter of 9.6 mm, the nozzle throat diameter of 8.14 mm, as well as the movable stroke of the adjustable cone. Keeping the cone top angle, α, and cone bottom diameter unchanged, the mass-flow rate of the primary flow

can be adjusted by moving the cone horizontally in the direction of the outlet of the diffuser of the ejector. A partially enlarged view of the adjustable cone is shown in fig. 2.

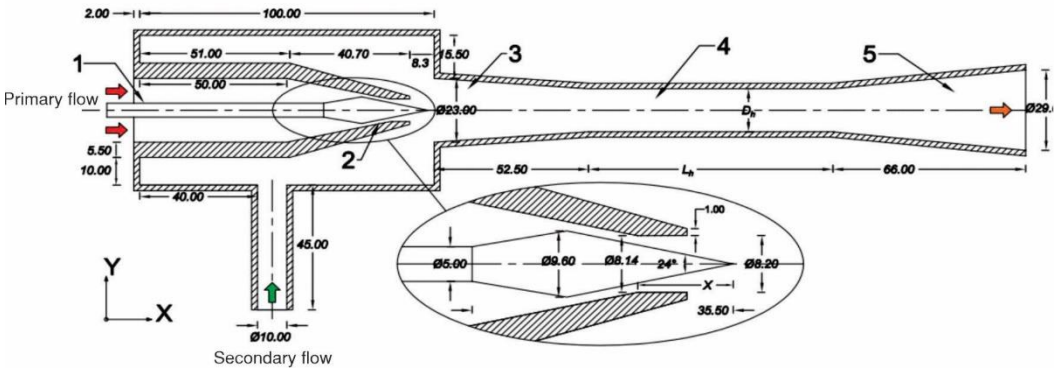

Figure 1. Sketch of adjustable ejector structure; *1 – adjustable cone, 2 – nozzle, 3 – suction chamber, 4 – mixing chamber, and 5 – diffuser*

When the tip of the adjustable cone is precisely located on the X-axis with its position at X = 93.3 mm (nozzle throat section), the moving distance of the adjustable cone is regarded as x = 0 mm. If the adjustable cone moves forward along the X-axis, each unique m value corresponds to a specific position of the adjustable cone, and this position information is marked and recorded by using the parameter spindle position (SP). Different adjustable cone strokes correspond to different cone positions as shown in tab. 1.

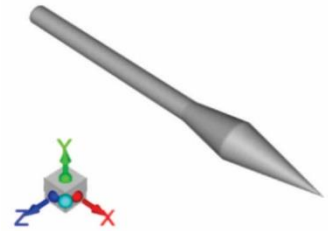

Figure 2. Partial view of the adjustable cone structure

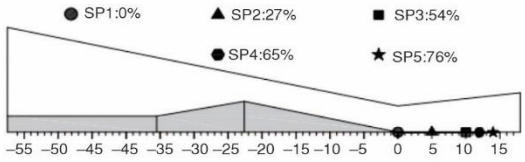

Figure 3. The position of adjustable cone for different cone diameter ratios

Table 1. Adjustable cone stroke and cone position table

Spindle position	SP_1	SP_2	SP_3	SP_4	SP_5
x [mm]	0	5	10	12	14

In this paper, cone diameter ratio (the ratio between diameter of adjustable cone and diameter of nozzle throat) is used to characterize the position of the adjustable cone. Cone diameter ratios are 0%, 27%, 54%, 65%, and 76%, respectively, as shown in fig. 3.

Numerical simulation

Turbulence model equations

Relevant studies show that the Realizable k-ε model can well reflect the change of flow field inside the ejector [11]. Consequently, this study adopts this model as its basis for analysis. The equations are as:

$$\frac{\partial(\rho k)}{\partial t}+\frac{\partial(\rho k u_i)}{\partial x_i}=\frac{\partial}{\partial x_j}\left[\left(\mu+\frac{\mu_t}{\sigma_k}\right)\frac{\partial k}{\partial x_j}\right]+G_k+G_b-\rho\varepsilon-Y_m \tag{1}$$

$$\frac{\partial(\rho\varepsilon)}{\partial t}+\frac{\partial(\rho\varepsilon u_i)}{\partial x_j}=\frac{\partial}{\partial x_j}\left[\left(\mu+\frac{\mu_t}{\sigma_\varepsilon}\right)\frac{\partial\varepsilon}{\partial x_j}\right]+\rho C_1 E\varepsilon-\rho C_2\frac{\varepsilon^2}{k+\sqrt{v\varepsilon}}+C_{1\varepsilon}\frac{\varepsilon}{k}C_3 \tag{2}$$

where G_k is the turbulent kinetic energy due to the laminar velocity gradient, G_b – the turbulent kinetic energy due to buoyancy, Y_m – the fluctuation due to diffusion in transition in compressible turbulence, and C_1, C_2, and $C_{1\varepsilon}$ are constants.

Boundary conditions

Setting adjustable ejector inlet and outlet boundary conditions, the primary flow and secondary flow R41/R1234yf mixed refrigerant mass ratio of 9:1 and 7:3, respectively. The inlet pressure of the primary flow is 1.4 MPa and the temperature is 353.15 K. The inlet pressure of the secondary flow is 0.2 MPa and the temperature is 288.15 K. The outlet pressure of the ejector is 0.3 MPa. The walls are adiabatic, impermeable, and slip-free boundary conditions, and the species transport model is turned on.

Grid independence study

In order to ensure the accuracy of the numerical simulation results, saving computational resources, and assess the reliability of the simulation results, grid-independence validation is carried out. As shown in fig. 4, the entrainment ratio is 0.688 when the grid number reaches 415304. Compared to the models with 384840 and 515375 grids, the variation of entrainment ratio is 0.14% and 1.6%, respectively. Therefore, the final choice is made to control the number of grids at 415304.

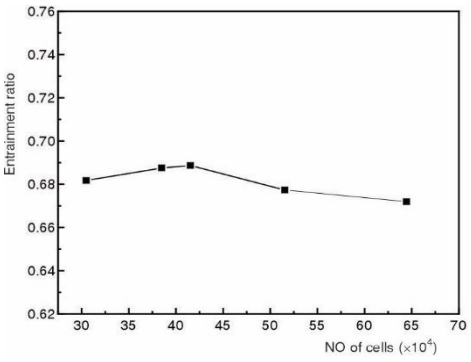

Figure 4. Grid-independence validation

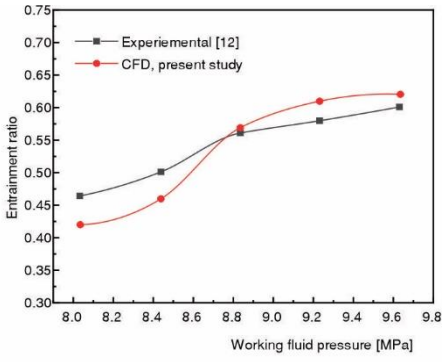

Figure 5. Error analysis of experiment and simulation values

Validation of the CFD model

Numerical simulation is carried out by keeping the simulated operating parameters consistent with the operating parameters in the experiments in [12]. The error analysis of the simulated and experimental values is shown in fig. 5, the errors between the simulated and experimental values of the ejector under five groups of operating conditions are –9.52%,

–8.70%, 1.75%, 4.92%, and 3.23%, respectively, and the maximum error is controlled within ±10%, which meets the requirements for use.

Results and discussion

The entrainment ratio is an important performance indicator of ejector performance. The entrainment ratio is defined as:

$$\mu = \frac{M_g}{M_s} \tag{3}$$

where M_g [kgs^{-1}] is the mass-flow rate of the secondary flow of the ejector and M_s [kgs^{-1}] – the mass-flow rate of primary flow.

Effect of refrigerant mix ratio on ejector performance

As shown in fig. 6(a), variation of ejector performance with different ratios of R41/R1234yf refrigerant blends as primary flow at mass-flow rates of 0.08 kg/s, 0.09 kg/s, 0.10 kg/s, and 0.11 kg/s, respectively, and a secondary flow pressure of 0.2 MPa. The entrainment ratio reaches a maximum value of 0.77 at R41/R1234yf refrigerant blend mass ratio of 9:1 and primary flow mass-flow rate of 0.11 kg/s.

As shown in fig. 6(b), variation of ejector performance with different ratios of R41/R1234yf refrigerant blends as secondary flow at mass-flow rates of 0.03 kg/s, 0.04 kg/s, 0.05 kg/s, and 0.06 kg/s, respectively, and a primary flow pressure of 0.2 MPa. The entrainment ratio reaches a maximum value of 0.85 at R41/R1234yf refrigerant blend mass ratio of 7:3 and secondary flow mass-flow rate of 0.06 kg/s.

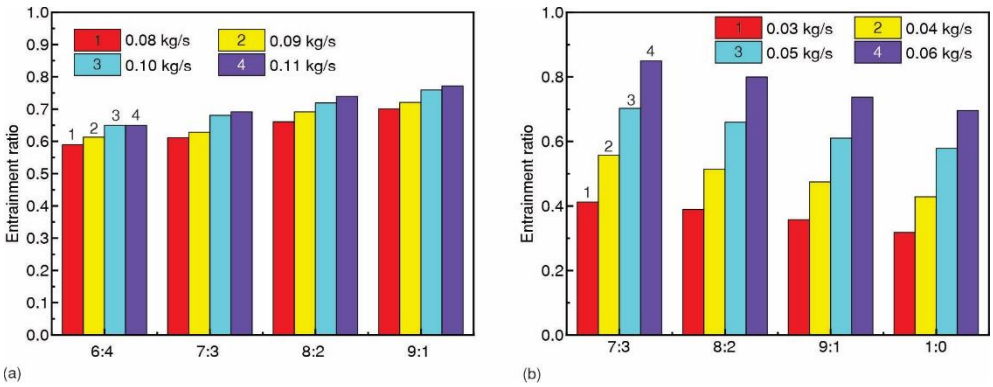

Figure 6. Effect of the ratio of mixed refrigerant in primary flow (a) and secondary flow (b) on the performance of the ejector

Therefore, in the subsequent work, the adjustable ejector inlet boundary conditions are set and the mass ratios of the R41/R1234yf refrigerant mix of primary flow and secondary flow are 9:1 and 7:3, respectively.

Effect of mixing chamber diameter on the performance of adjustable ejector

As shown in fig. 7, the velocity profile within the adjustable is presented when cone diameter ratio is 0%, length of mixing chamber is L_h = 88 mm, and the diameter is within the

range of 14.7-18.7 mm. Secondary shock wave phenomenon is observed at the inlet of the diffuser, and the strength of the secondary shock wave reduces as diameter of mixing chamber increases. As diameter of the mixing chamber increases, secondary shock wave gradually moves toward nozzle outlet. When the mixing chamber diameter is 16.7 mm, secondary shock wave almost disappears. This phenomenon is due to the fact that as the diameter of the mixing chamber increases, velocity equilibrium between primary flow and secondary flow becomes worse, expansion time of the primary flow is shortened, and velocity drop becomes larger, leading to gradual shortening of the shock wave chain in the flow field and the increase of momentum loss in the mixing chamber. It is also observed that the flow velocity of the secondary flow changes appreciably, driving the secondary flow into the receiving chamber is strongly related to the formation of shock wave and the diameter of the mixing chamber.

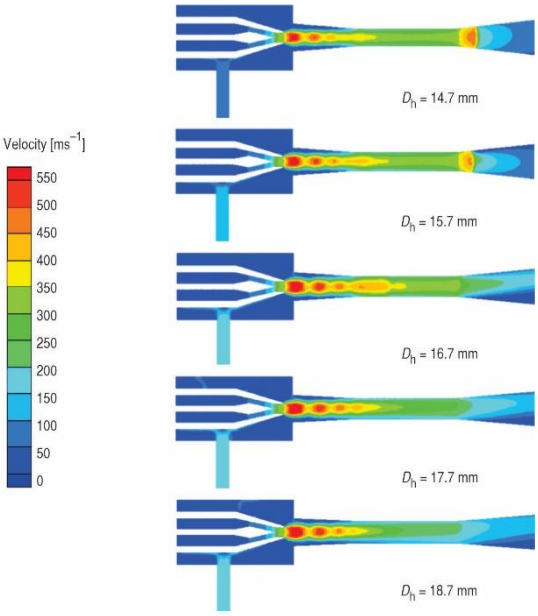

Figure 7. Velocity profile of the adjustable ejector for different mixing chamber diameters

Figure 8 shows distribution of pressure *vs*. Mach number on centre axis of the adjustable ejector for five different mixing chamber diameters by keeping cone diameter ratio constant at 0%. From fig. 8, it can be seen that pressure has a negative correlation trend with Mach number. When mixing chamber diameter is constant, with the increase of axial distance, Mach number in mixing chamber shows a significant decreasing trend, which proves that primary flow and secondary flow in mixing chamber have reached the purpose of mixing. When diameter of mixing chamber gradually increases, Mach number in mixing chamber first rises and then decreases, and in vicinity of the inlet of the diffuser, magnitude of the Mach number fluctuations gradually decreases. Under effect of a combination of factors, change of the fluid flow rate and formation of shock waves appear with the corresponding changes in fig. 7.

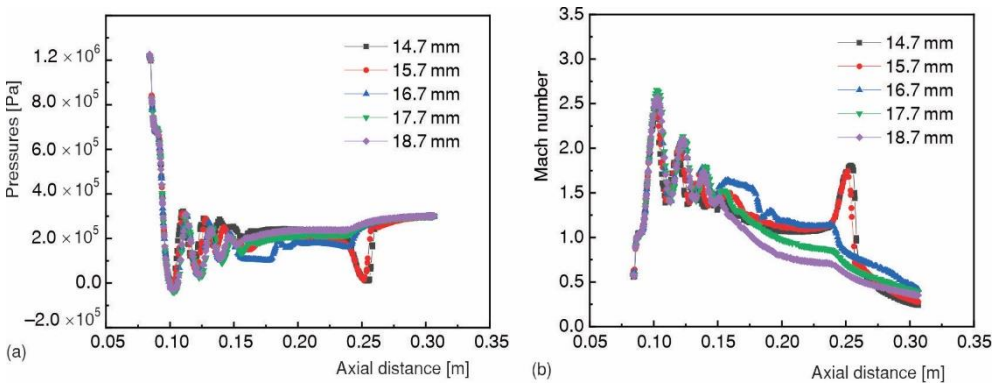

Figure 8. Effect of mixing chamber diameter on pressure (a) *vs*. Mach number (b)

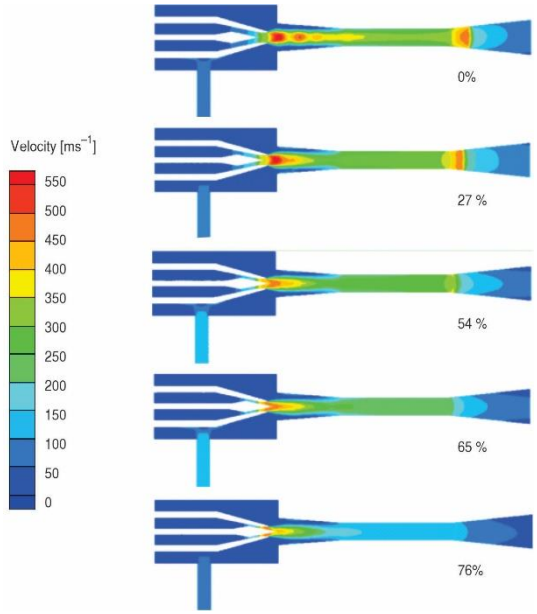

Figure 9. Velocity profile of the adjustable ejector with different cone diameter ratios

Figure 9 shows the velocity profile inside the adjustable ejector for a cone diameter ratio of 0% to 76% and a mixing chamber diameter of 14.7 mm. From fig. 9, it is observed that with the increase of the cone diameter ratio, due to the change of nozzle outlet cross-sectional area and influence of the shape of the adjustable cone, primary flow at the nozzle outlet changes from a high-speed concentration to a lower velocity and flows out at a wider angle. Secondary shock wave at the inlet of the diffuser gradually disappears. At the same time, it is observed that space for secondary flow to enter the suction chamber increases, and the flow rate of secondary flow increases and then decreases with the increase of the cone diameter ratio, which proves that the performance of the ejector is changed.

Figure 10 shows the distribution of pressure versus Mach number on centre axis of adjustable ejector for five different cone diameter ratios, keeping mixing chamber diameter constant at 14.7 mm. From fig. 10, it can be seen that pressure has a negative correlation trend with Mach number. With increase of cone diameter ratio, flow area of fluid decreases, mass-flow rate of primary flow decreases, kinetic energy of fluid is converted into pressure energy, pressure at nozzle outlet increases, and pressure fluctuation at nozzle outlet and diffuser inlet decreases gradually. This phenomenon is highly related to shock wave phenomenon observed at nozzle outlet and diffuser inlet of the adjustable ejector in fig. 9.

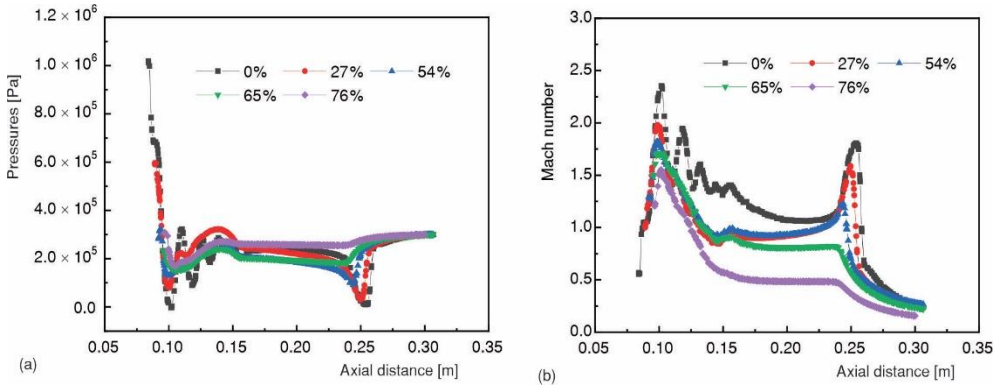

Figure 10. Effect of cone diameter ratio on pressure (a) *vs.* Mach number (b)

As shown in fig. 11, under the condition of same cone diameter ratio, entrainment ratio shows a tendency of increasing and then decreasing with increase of mixing chamber diameter. Specifically, at a cone diameter ratio of 0%, when mixing chamber diameter increases from 14.7 mm to 17.7 mm, entrainment ratio increases from 0.253 to 0.409,

reaching the maximum value. When the mixing chamber diameter continues to increase to 18.7 mm, entrainment ratio decreases to 0.38. When cone diameter ratio is 76%, tendency to show this change is more obvious, and maximum change in entrainment ratio can reach 49.5%. According to the data analysis of figs.7 and 8, as mixing chamber diameter increases, flow path constraint effect of nozzle outlet weakens, flow resistance of fluid in suction chamber weakens, back flow of fluid at suction chamber weakens, and effect of shock wave gradually weakens. Moreover, increase of the mixing chamber provides sufficient space for primary flow and secondary flow to be fully mixed. Therefore, entrainment ratio of adjustable ejector rises. However, when diameter of mixing chamber reaches specific value, if diameter of mixing chamber continues to increase, velocity balance between primary flow and secondary flow will become worse and shear action between mainstream and secondary flow will also weaken. At this time, expansion time of primary flow is shortened, speed drop amplitude increases, shock chain in flow field is gradually shortened, and momentum loss in mixing chamber increases. Eventually, this leads to reduction in entrainment rate of adjustable ejector. In the case of a higher cone diameter ratio, the role of the cone part is more prominent. Its shape is more important for controlling gas flow. Therefore, it leads to a greater variation range of entrainment ratio of the adjustable ejector.

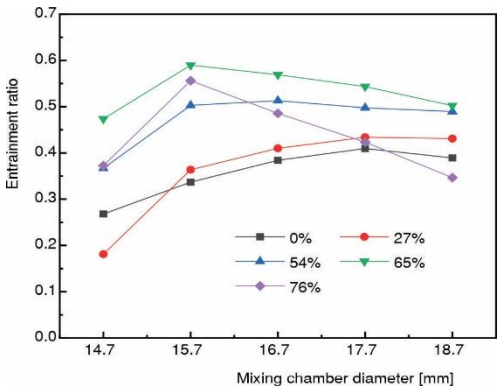

Figure 11. Effect of mixing chamber diameter on entrainment ratio

In addition, the entrainment ratio of the adjustable ejector generally shows a trend of first rising and then falling with the increase of the cone diameter ratio. When the cone diameter ratio reaches 65%, the adjustable ejectors with different mixing chamber diameters show the maximum entrainment ratio. The adjustable ejector with a mixing chamber diameter of 15.7 mm and a cone diameter ratio of 65% has the maximum entrainment ratio with a value of 0.59. Further observation shows that as the cone diameter ratio increases, the maximum entrainment ratio obtained by the adjustable ejector with different diameter mixing chambers presents a shifting trend towards the direction of a smaller mixing chamber diameter. As the cone diameter ratio increases from 0% to 76%, the mixing chamber diameters corresponding to the maximum entrainment ratio are 17.7 mm, 17.7 mm, 16.7 mm, 15.7 mm, and 15.7 mm, respectively. Combined with the analysis of figs. 9 and 10, as cone diameter ratio increases, although mass-flow rate of primary flow and fluid velocity at nozzle continuously decrease, degree of expansion of fluid at nozzle outlet and strength of shock wave are correspondingly weakened. Moreover, when secondary flow enters suction chamber, it has more space and can be fully mixed with primary flow. Therefore, mass-flow rate of secondary flow is not significantly reduced, and entrainment ratio increases. However, if cone diameter ratio continues to increase, due to change of cross-sectional area of nozzle outlet and influence of shape of adjustable cone, primary flow at nozzle outlet changes from high-speed concentration to spraying out at a lower speed and a wider angle. This makes back flow effect of fluid in suction chamber significantly enhanced. The flow state of fluid may change, leading to flow separation or other flow phenomena, which will cause entrainment ratio to start decreasing.

Effect of mixing chamber length on the performance of adjustable ejector

As shown in fig. 12, the velocity profile inside adjustable ejector is presented when the cone diameter ratio is 0%, diameter of the mixing chamber is D_h = 14.7 mm, and the length is within the range of 24-220 mm. As can be seen from fig. 12, when the length of the mixing chamber is short, fluid velocity near the wall of the mixing chamber is lower, while fluid velocity at the center is higher. Under such circumstances, the mixing of primary flow and secondary flow is insufficient. As length of mixing chamber increases, process of primary flow deceleration and pressure rise is prolonged. The mixing process between the primary flow and the secondary flow in the mixing chamber is gradually stabilizes, and the loss of fluid mechanical energy is reduced. Continuing to increase the length of the mixing chamber will increase the resistance to flow of the fluid, and loss of mechanical energy increases. Two large fluctuations in fluid velocity are simultaneously observed, displaying pronounced shock wave phenomena, the first fluctuation emerges in proximity to the nozzle outlet. When supersonic primary flow suddenly increases in flow area, it will expand and accelerate. Then, in the mixing chamber, it will conduct velocity equalization and energy exchange with low-speed secondary flow. The second fluctuation appears at the upstream position of the diffuser. In order to overcome back pressure at the ejector outlet, the speed of supersonic mixture drops sharply. When the length of the mixing chamber is 24 mm, there is an obvious shock wave phenomenon at the inlet section of the diffuser. As the length of the mixing chamber increases, secondary shock wave at inlet of the diffuser gradually weakens. When the mixing chamber length is 220 mm, the secondary shock wave almost disappears, and shock wave chain also disappears in the mixing chamber.

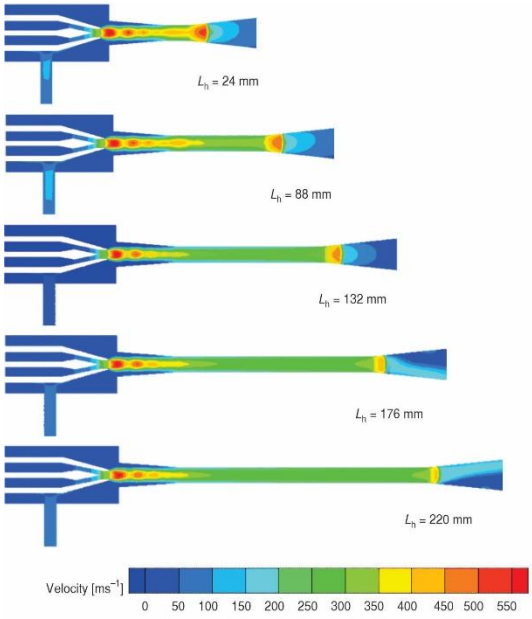

Figure 12. Velocity profile of adjustable ejector with different mixing chamber lengths

Figure 13 shows the influence of different lengths of mixing chamber on pressure and Mach number on the central axis of adjustable ejector when the cone diameter ratio is 0% and the diameter of mixing chamber is 14.7 mm. It can be observed in fig. 13(a) that as the length of the mixing chamber increases, the minimum pressure in mixing chamber shows a gradually increasing trend. Furthermore, pressure fluctuation at the inlet of the diffuser chamber gradually attenuates, and shock wave located here is also gradually weakening. As shown in fig. 12, the shock wave phenomenon at the inlet of the diffuser varies correspondingly with the increase in the length of the mixing chamber. This is because in a shorter mixing chamber, the time and space for fluid to flow are limited, resulting in a relatively short time for the conversion of velocity potential energy to static pressure energy. Conversely, when the mixing chamber is longer, the fluid has more time and space for the energy conversion process. As shown in fig. 13(b), the Mach number of fluid at outlet of the mixing chamber is inversely proportional to

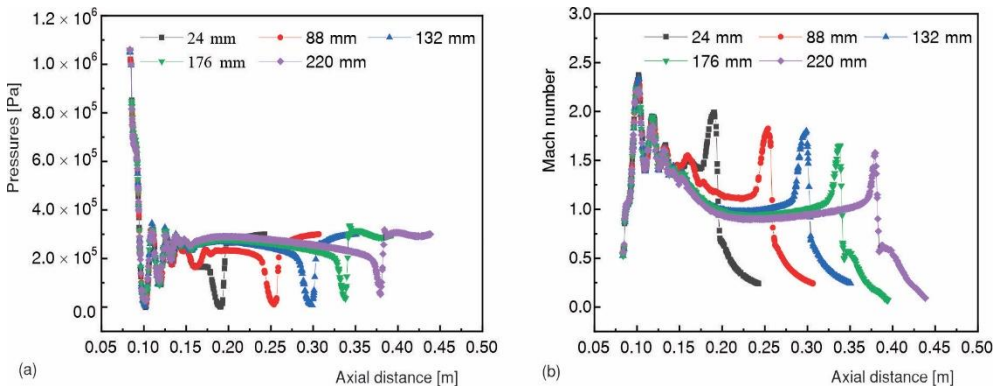

Figure 13. Effect of mixing chamber length on pressure (a) *vs.* Mach number (b)

length of mixing chamber. When length of mixing chamber increases, the influence of environmental pressure on mixed fluid in diffuser chamber will increase accordingly, which in turn leads to a more obvious back flow phenomenon in diffuser chamber. Consequently, the fluid flow exhibits an unstable state. Therefore, as the length of mixing chamber continues to increase, the normal working range of adjustable ejector will gradually narrow.

When the diameter of mixing chamber is D_h = 14.7 mm, the influence of length of mixing chamber on entrainment ratio of adjustable ejector is shown in fig. 14. Under the condition of the same cone diameter ratio, with the increase of the length of the mixing chamber, the entrainment ratio of the adjustable ejector shows a trend of first rising and then falling. Under different cone diameter ratios, adjustable ejector always shows the best performance when length of its mixing chamber is 88 mm. When the cone diameter ratio of adjustable ejector with mixing chamber length of 88 mm increases from 0% to 76%, its entrainment ratios are 0.267, 0.302, 0.478, 0.581, and 0.624, respectively. According to the data analyses of figs. 12 and 13, under the condition of the same cone diameter ratio, when length of mixing chamber is short, fluctuation amplitude of pressure and velocity of fluid in mixing chamber is too large. The mixing of the primary flow and secondary flow is significantly inadequate. Mixing chamber does not play an effective mixing role for two fluids, which affects performance of adjustable ejector. When the length of the mixing chamber is increased to 88 mm, the mixing chamber can achieve the full mixing of the primary flow and the secondary flow in the most effective way. At the same time, the diffuser chamber also shows better pressure recovery ability. Therefore, the entrainment ratio of the adjustable ejector is improved well. However, when the length of the mixing chamber is further increased to 220 mm, the drag losses increase accordingly, causing the energy loss of the mixed fluid to continuously increase. In this case, the performance of the ejector will decline.

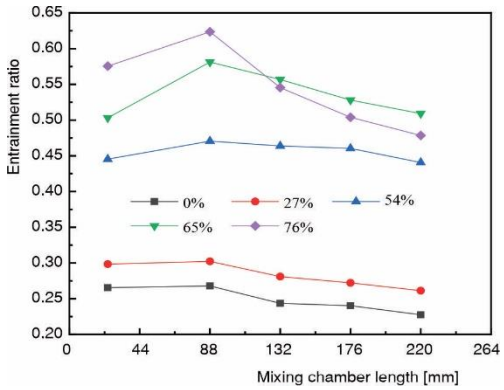

Figure 14. Effect of mixing chamber length on entrainment ratio

For the length of mixing chamber in range of 44-88 mm, the entrainment ratio gradually increases as the cone diameter ratio increases. However, for the length in range of 132-220 mm, the entrainment ratio shows a trend of first rising and then falling as the cone diameter

ratio increases, and the entrainment ratio reaches peak when the cone diameter ratio is 65%. The reason for this trend is that as the cone diameter ratio increases, the flow velocity of the primary flow decreases. Consequently, the primary and secondary flows have a longer period of time to blend thoroughly within the mixing chamber. Therefore, the entrainment ratio of the adjustable ejector experiences an enhancement. However, if the length of mixing chamber is too long, fluid's irreversible loss will increase, and the ability to overcome back pressure will weaken, which may lead to back flow. At this time, it is possible that as the cone diameter ratio increases, the entrainment ratio of the adjustable ejector may undergo a decrease.

Conclusions

This study selects the R41/R1234yf refrigerant gas as the working medium. The inlet pressure of the primary flow is 1.4 MPa and the temperature is 353.15 K. The inlet pressure of the secondary flow is 0.2 MPa and the temperature is 288.15 K. The outlet pressure of the ejector is 0.3 MPa. The influence of the structural parameters of the mixing chamber on the performance of the adjustable ejector under different cone diameter ratios is studied. The main conclusions are as follows.

- Within the range of mixing chamber diameter from 14.7 mm to 18.7 mm, when the cone diameter ratio is the same, the entrainment ratio of adjustable ejector shows a trend of first increasing and then decreasing with the increase of mixing chamber diameter. There exists an optimal mixing chamber diameter for adjustable ejector, which can make ejector performance reach the best state. Specifically, when the cone diameter ratio is 65% and the mixing chamber diameter is 15.7 mm, the entrainment rate reaches the maximum value of 0.59.
- Under the condition of same cone diameter ratio, as the length of mixing chamber increases from 24 mm to 220 mm, the entrainment ratio of adjustable ejector shows a trend of first rising and then falling. When the length of mixing chamber of ejector is 88 mm and the cone diameter ratio is 76%, the ejector achieves its peak entrainment ratio of 0.624.

Acknowledgment

The authors are grateful to the financial support from National Natural Science Foundation of China (NSFC) (No. 51566014) and Basic Science and Technology Projects of the Directly Administered Universities in Inner Mongolia Autonomous Region.

References

[1] Al-Khalidy, N., Experimental Investigation of Solar Concentrating Collectors in a Refrigerant Ejector Refrigeration Machine, *International Journal of Energy Research, 21* (1997), 12, pp. 1123-1131
[2] Aligolzadeh, F., Hakkaki-Fard, A., A Novel Methodology for Designing a Multi-Ejector Refrigeration System, *Applied Thermal Engineering, 151* (2019), Mar., pp. 26-37
[3] Rostamnejad, H., Zare, V., Performance Improvement of Ejector Expansion Refrigeration Cycles Employing a Booster Compressor Using Different Refrigerants: Thermodynamic Analysis and Optimization, *International Journal of Refrigeration, 101* (2019), May, pp. 56-70
[4] Liang, X., *et al*., Thermodynamic Analysis of a Novel Combined Double Ejector-Absorption Refrigeration System Using Ammonia/Salt Working Pairs Without Mechanical Pumps, *Energy, 185* (2019), Oct., pp. 895-909
[5] Wang, Z., *et al*., Influence of Mixing Chamber Structure on Entrainment Ratio of Steam Ejector: A Simulation Study, *Chinese Journal of Vacuum Science and Technology, 40* (2020), 2, pp. 180-186
[6] Jia, Y., Wenjian, C., Area Ratio Effects to the Performance of Air-Cooled Ejector Refrigeration Cycle with R134a Refrigerant, *Energy Conversion and Management, 53* (2012), 1, pp. 240-246
[7] Yan, J., *et al*., Geometry Parameters Effect for Air-Cooled Ejector Cooling Systems with R134a Refrigerant, *Renewable Energy, 46* (2012), Oct., pp. 155-163

[8] Varga, S., *et al*., Influence of Geometrical Factors on Steam Ejector Performance – A Numerical Assessment, *International Journal of Refrigeration, 32* (2009), 7, pp. 1694-1701
[9] Li, H., *et al*., Performance Characteristics of R1234yf Ejector-Expansion Refrigeration Cycle, *Applied Energy, 121* (2014), May, pp. 96-103
[10] Yang, M., *et al*., Flow Characteristics in Ejector by Using Azeotropic Mixed Refrigerant, J*ournal of Henan University of Science & Technology, Natural Science, 41* (2020), 4, p. 67
[11] Zhang, X., *et al*., Research Progress of Ejector Geometric Optimization and Refrigeration Applications, *Journal of Chemical Engineering of Chinese Universities, 34* (2020), 2, pp. 277-289
[12] Zhu, C., Performance Study on Ejector in CO_2 Ejector Absorption Refrigeration System, Ph. D. thesis, Inner Mongolia University of Science and Technology, Baotou, China, 2017

Paper submitted: July 14, 2024
Paper revised: August 23, 2024
Paper accepted: August 31, 2024